











First direct carbon abundance measured at $z > 10$ in the lensed galaxy MACS0647–JD

TIGER YU-YANG HSIAO ^{1,2,3} MICHAEL W. TOPPING ⁴ DAN COE ^{3,5,2} JOHN CHISHOLM ⁶ DANIELLE A. BERG ⁶
ABDURRO'UF ^{2,3} JAVIER ÁLVAREZ-MÁRQUEZ ⁷ ROBERTO MAIOLINO ^{8,9,10} PRATIKA DAYAL ¹¹ AND
LUKAS J. FURTAK ¹²

¹Center for Astrophysics | Harvard & Smithsonian, 60 Garden Street, Cambridge, MA 02138, USA

²Center for Astrophysical Sciences, Department of Physics and Astronomy, The Johns Hopkins University, 3400 N Charles St. Baltimore, MD 21218, USA

³Space Telescope Science Institute (STScI), 3700 San Martin Drive, Baltimore, MD 21218, USA

⁴Department of Astronomy / Steward Observatory, University of Arizona, 933 N Cherry Ave, Tucson, AZ 85721

⁵Association of Universities for Research in Astronomy (AURA), Inc. for the European Space Agency (ESA)

⁶Department of Astronomy, University of Texas at Austin, 2515 Speedway, Austin, Texas 78712, USA

⁷Centro de Astrobiología (CAB), CSIC-INTA, Ctra. de Ajalvir km 4, Torrejón de Ardoz, E-28850, Madrid, Spain

⁸Kavli Institute for Cosmology, University of Cambridge, Madingley Road, Cambridge CB3 0HA, UK

⁹Cavendish Laboratory, University of Cambridge, 19 JJ Thomson Avenue, Cambridge CB3 0HE, UK

¹⁰Department of Physics and Astronomy, University College London, Gower Street, London WC1E 6BT, UK

¹¹Kapteyn Astronomical Institute, University of Groningen, 9700 AV Groningen, The Netherlands

¹²Physics Department, Ben-Gurion University of the Negev, P.O. Box 653, Be'er-Sheva 84105, Israel

ABSTRACT

Investigating the metal enrichment in the early universe helps us constrain theories about the first stars and study the ages of galaxies. The lensed galaxy MACS0647–JD at $z = 10.17$ is the brightest galaxy known at $z > 10$. Previous work analyzing JWST NIRSpec and MIRI data yielded a direct metallicity $12 + \log(\text{O}/\text{H}) = 7.79 \pm 0.09$ ($\sim 0.13 Z_{\odot}$) and electron density $\log(n_e/\text{cm}^{-3}) = 2.9 \pm 0.5$, the most distant such measurements to date. Here we estimate the direct C/O abundance for the first time at $z > 10$, finding a sub-solar $\log(\text{C}/\text{O}) = -0.44_{-0.07}^{+0.06}$. This is higher than other $z > 6$ galaxies with direct C/O measurements, likely due to higher metallicity. It is also slightly higher than galaxies in the local universe with similar metallicity. This may suggest a very efficient and rapid burst of star formation, a low effective oxygen abundance yield, or the presence of unusual stellar populations including supermassive stars. Alternatively, the strong C III] $\lambda\lambda 1907, 1909$ emission ($14 \pm 3 \text{ \AA}$ rest-frame EW) may originate from just one of the two component star clusters JDB ($r \sim 20 \text{ pc}$). Future NIRSpec IFU spectroscopic observations of MACS0647–JD will be promising for disentangling C/O in the two components to constrain the chemistry of individual star clusters just 460 Myr after the Big Bang.

Keywords: Early universe (435), Chemical abundances (224), Metallicity (1031), Galaxies (573), High-redshift galaxies (734), Galaxy spectroscopy (2171)

1. INTRODUCTION

The first generation of stars (Pop III) are believed to contain no elements heavier than helium (dubbed metals; e.g., Barkana & Loeb 2001; Klessen & Glover 2023). The quest to find Pop III stars is ongoing and will help us understand how the first metals were built

up. Since directly detecting Pop III stars is challenging, understanding the chemical abundance of heavy elements in high-redshift galaxies could be key to constraining the properties of Pop III stars. Specifically, oxygen and carbon are the most abundant metals in the universe. Oxygen is generated heavily from the death of massive stars ($M > 8 M_{\odot}$) through core-collapse supernovae (CCSN), soon after the onset of star formation (e.g., Nomoto et al. 2013). Carbon is enriched not only via CCSN but also during the asymptotic giant branch (AGB) phase of intermediate-mass stars which have sig-

nificantly longer lifetimes than massive stars that undergo CCSN (e.g., Kobayashi et al. 2011; Karakas & Lattanzio 2014; Kobayashi et al. 2020). Therefore, the C/O ratio can be diagnostic of galaxy ages, increasing at ages $\gtrsim 100$ Myr. Other astrophysical processes also affect C/O. For instance, the C/O ratio is sensitive to supernova-driven outflows (Berg et al. 2019), star-formation history (SFH) (Berg et al. 2020), and the initial mass function (IMF). High- z galaxies are thought to have a top-heavy initial mass function (IMF) (Inayoshi et al. 2022), favoring the formation of more massive stars and a lower C/O. Meanwhile, the oxygen abundance, O/H, traces the integrated star formation history. Comparisons of the C/O and O/H abundances constrain the relatively recent star formation history (through C/O) versus the total star formation in the galaxy (O/H).

The JWST, a groundbreaking space telescope, opens the window to spectroscopically study the chemical abundances in high redshift galaxies in high redshift galaxies ($z > 6$) thanks to its unique wavelength coverage, unparalleled sensitivity, and spatial resolution in the rest-frame optical (e.g., Arellano-Córdova et al. 2022; Jones et al. 2023; Isobe et al. 2023; D’Eugenio et al. 2023; Bunker et al. 2023; Maiolino et al. 2023; Cameron et al. 2023; Hsiao et al. 2023a; Topping et al. 2024; Castellano et al. 2024; Hsiao et al. 2024). Most of these galaxies have low metallicity ($Z < 0.2 Z_{\odot}$) and low C/O ratios ($\log(\text{C/O}) < -0.6$) as expected for low-mass galaxies that are heavily impacted by stellar feedback from relatively recent star formation (Arellano-Córdova et al. 2022; Jones et al. 2023; Isobe et al. 2023; Topping et al. 2024). Surprisingly, a high C/O ratio of $\log(\text{C/O}) > -0.08$ was discovered in galaxy GS-z12 at $z = 12.5$, and was interpreted as the heritage of Pop III stars (D’Eugenio et al. 2023), since supermassive stars (e.g. Pop III stars) could have different abundance patterns than the typical massive stars. Regarding other $z > 10$ galaxies, GHZ2 ($z = 12.34$) has a subsolar carbon abundance of $\log(\text{C/O}) \sim -0.94$ to -0.53 (Castellano et al. 2024), and $\log(\text{C/O}) > -0.78$ is estimated in GN-z11 ($z = 10.6$; Cameron et al. 2023). However, all previous C/O measurements at $z > 10$ were derived from assumed electron temperature (T_e) and/or assumed electron density (n_e) due to the lack of resolved temperature-sensitive and density-sensitive line ratios. To reduce the uncertainty, direct C/O measurements are needed to truly understand how carbon is enriched.

MACS0647–JD, a lensed galaxy at $z = 10.17$, provides a promising laboratory for the C/O abundance in the early universe. It is triply lensed to three images: JD1, JD2, and JD3, with magnifications of 8, 5.3, and 2.2, respectively. Given its high magnification (F200W

AB mag 25.0), Hsiao et al. (2023b) studied JWST NIRCam imaging, which resolved MACS0647–JD into two small components JDA and JDB, suspected to be a possible galaxy merger, plus a possible third companion C (~ 3 kpc away). JDA is larger (deensed radius of $r = 70 \pm 24$ pc), brighter, and bluer, likely due to its young stellar population (~ 50 Myr old) and lack of dust. In contrast, JDB, is smaller (deensed effective radius of $r = 20^{+8}_{-5}$ pc), and is redder, likely due to an older stellar population (~ 100 Myr old) and mild dust ($A_V \sim 0.1$ mag). An additional possible companion JDC is nearby, 3 kpc away. Later, Hsiao et al. (2023a) and Hsiao et al. (2024) reported JWST Cycle 1 NIRSpec prism spectroscopy and JWST Cycle 2 MIRI IFU spectroscopy. The auroral line [O III] $\lambda 4363$ and [O III] $\lambda 5008$ were detected in NIRSpec prism and MIRI IFU spectroscopy, respectively, yielding the first direct metallicity measurement at $z > 10$ of $12 + \log(\text{O/H}) = 7.79 \pm 0.09$ (Hsiao et al. 2024). Here, we combine the C III] $\lambda\lambda 1907, 1909$ detections from NIRSpec prism data with the [O III] $\lambda 4363$ and [O III] $\lambda 5008$ observations from NIRSpec and MIRI to provide the first direct C/O measurement at $z > 10$. These data explore the enrichment of stellar populations within galaxies in the first few hundred Myr of cosmic time.

Throughout this article, we adopt solar abundance ratios $12 + \log(\text{O/H}) = 8.69$ and $\log(\text{C/O}) = -0.23$ (Asplund et al. 2021). Lensing magnifications of 8.0 and 5.3 are adopted for JD1 and JD2, respectively (Hsiao et al. 2023b). Magnification uncertainties ($\sim 15\%$) do not affect line flux ratios or derived abundance ratios. Where needed, we adopt the *Planck* 2018 flat Λ CDM cosmology (Planck Collaboration et al. 2020) with $H_0 = 67.7$ km s $^{-1}$ Mpc $^{-1}$, $\Omega_M = 0.31$, and $\Omega_{\Lambda} = 0.69$, for which the universe is 13.8 billion years old and $z = 10.17$ is 460 Myr after the Big Bang.

2. DATA AND MEASUREMENT

This article makes use of the NIRCam (Rieke et al. 2005, 2023) and NIRSpec (Jakobsen et al. 2022; Ferruit et al. 2022; Böker et al. 2023) observations of JWST Cycle 1 program GO 1433 (PI Coe) and MIRI (Rieke et al. 2015; Wright et al. 2015, 2023) observations of JWST Cycle 2 program GO 4246 (PI Abdurro’uf). Both GO 1433 and GO 4246 observed MACS0647–JD. The data are publicly available on MAST.¹

2.1. NIRCam, NIRSpec, and MIRI

¹ <https://mast.stsci.edu/search/ui/#/jwst>
DOI:10.17909/wpys-ap03, DOI:10.17909/re1k-jt10

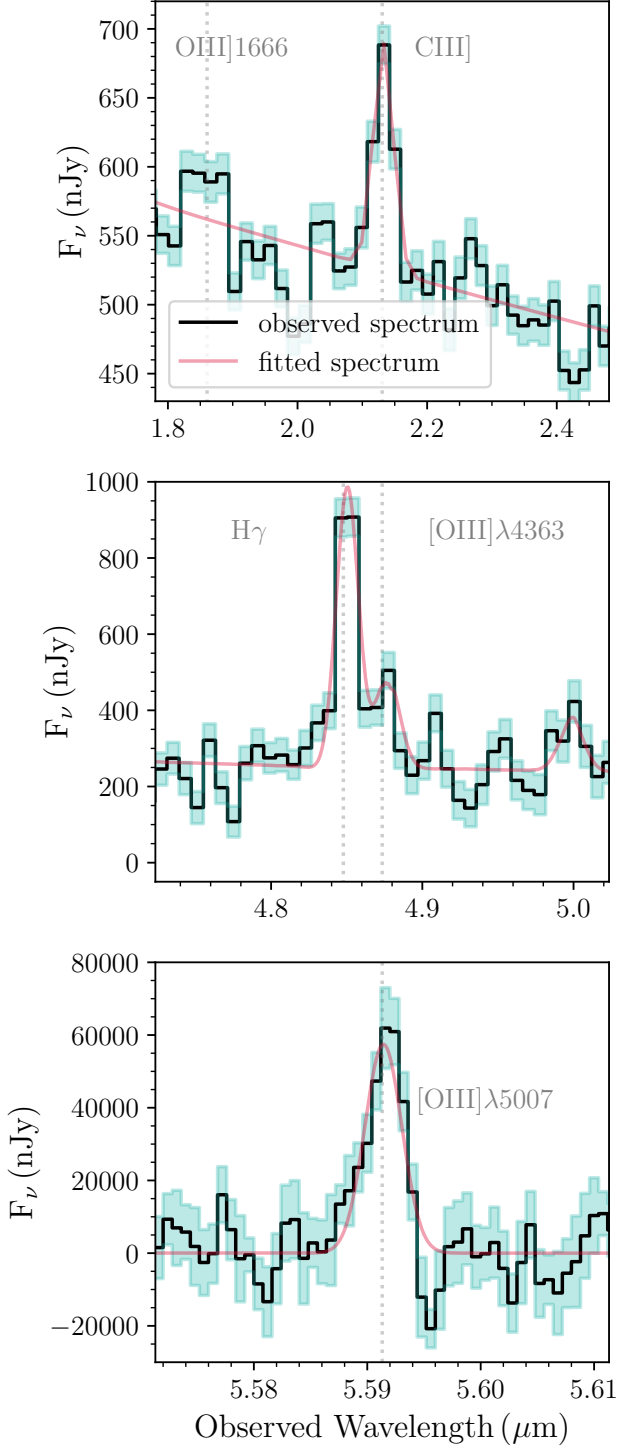


Figure 1. Emission lines used in this paper, including C III] $\lambda\lambda 1907, 1909$ (top panel), [O III] $\lambda 4363$ (middle panel), and [O III] $\lambda 5008$ (bottom panel). C III] $\lambda\lambda 1907, 1909$ and [O III] $\lambda 4363$ shown are stacked NIRSpectra with total magnification $\mu = 26.6$, while [O III] $\lambda 5008$ is the MIRI observation of JD1 with $\mu = 8$. The black lines show the observed spectrum and the red lines indicate the fit to the spectra and emission lines.

Table 1. Emission lines, lines ratios, and physical properties estimated for MACS0647–JD.

Emission Line Fluxes (10^{-19} erg/s/cm 2)	
C III] $\lambda\lambda 1907, 1909^a$	25 ± 2
[O III] $\lambda 4363^a$	5.6 ± 0.5
[O III] $\lambda 5008^b$	226 ± 21
Emission Line Ratios	
[O III] $\lambda 5008 / \lambda 4363^b$	40 ± 5
$O32^b = [\text{O III}] \lambda 5008 / [\text{O II}] \lambda 3727$	17 ± 2
$H\alpha / H\gamma^b$	5.5 ± 0.7
$R3^b = [\text{O III}] \lambda 5008 / H\beta$	6.9 ± 1.0
C III] $\lambda\lambda 1907, 1909 / [\text{O III}] \lambda 5008$	0.11 ± 0.01
Physical Properties	
$12 + \log(\text{O}/\text{H})^b$	7.79 ± 0.09
$\log(U)^b$	-1.9 ± 0.1
$T_e([\text{O III}])(\text{K})^b$	17000 ± 1000
$\log(n_e)^c$	2.9 ± 0.5
C ICF	1.10 ± 0.04
$\text{C}^{2+} / \text{O}^{2+}$	0.33 ± 0.05
$\log(\text{C}/\text{O})$	$-0.44^{+0.06}_{-0.07}$

^aCorrected for flux losses to match MIRI IFU.

^bHsiao et al. (2024)

^cAbdurro'uf et al. (2024).

NIRCam imaging was obtained in 7 filters, including 6 wide-band filters, F115W, F150W, F200W, F277W, F356W, and F444W, and a medium band, F480M, spanning 1–5 μm . Exposure times were 2104 s in each filter and twice that in F200W. All NIRCam data were reduced using the STScI JWST pipeline² (Bushouse et al. 2023) and GRIZLI (Brammer et al. 2022). In short, the pipeline performs corrections for $1/f$ noise striping and masks “snowballs”³ and “wisps”⁴ in each NIRCam exposure and then drizzle-combines all exposures to a common $0''.02$ pixel grid. Details on the NIRCam observations, data reduction, and photometric analysis of MACS0647–JD, including properties of the two individual components JDA and JDB, may be found in Hsiao

² <https://github.com/spacetelescope/jwst>

³ <https://jwst-docs.stsci.edu/data-artifacts-and-features/snowballs-and-shower-artifacts>

⁴ <https://jwst-docs.stsci.edu/jwst-near-infrared-camera/nircam-instrument-features-and-caveats/nircam-claws-and-wisps>

et al. (2023b). Updated photometry was presented in Hsiao et al. (2023a). In this article, we use the measured flux densities of F200W 368 nJy and F444W 317 nJy for MACS0647–JD1 to correct the flux losses between NIRSpec MSA prism spectroscopy and MIRI IFU spectroscopy (see §2.2).

NIRSpec multi-object spectroscopy (MOS) was performed using the microshutter assembly (MSA; Kutyrev et al. 2008; Rawle et al. 2022) to observe MACS0647–JD with the low-resolution prism ($R \sim 30 - 300$; $0.6 - 5.3 \mu\text{m}$) with 3.6 hours exposure time split between two visits (Hsiao et al. 2023a). Obs 23 performed standard 3-slitlet nods, while Obs 21 obtained data in single slitlets with two dithers. Briefly, NIRSpec Level 1 data products were retrieved from MAST and were processed with the STScI JWST pipeline version 1.9.2 and MSAEXP⁵ version 0.6.0, to correct for $1/f$ noise and mask snowballs. For the single-slitlet data, we subtract 2D background spectra from a nearby slit that observed a relatively blank region of the image. Full details of NIRSpec data reduction and background subtraction can be found in Hsiao et al. (2023a).

In the final reduced and stacked spectrum of MACS0647–JD, seven emission features were detected, including C III] $\lambda\lambda 1907, 1909$, [O II] $\lambda 3727$, [Ne III] $\lambda 3869$, [Ne III] $\lambda 3968$, H δ $\lambda 4101$, H γ $\lambda 4340$, and the auroral line [O III] $\lambda 4363$ (Hsiao et al. 2023a). In this article, we use emission line fluxes of the unresolved doublet C III] $\lambda\lambda 1907, 1909$ of $(428_{-35}^{+34}) \times 10^{-20} \text{ erg s}^{-1} \text{ cm}^{-2}$ and [O III] $\lambda 4363$ of $(62 \pm 5) \times 10^{-20} \text{ erg s}^{-1} \text{ cm}^{-2}$ measured from the stacked spectrum of four prism observations (including two on JD1 ($\mu_{\text{JD1}} = 8$) and two on JD2 ($\mu_{\text{JD2}} = 5.3$)), with a total magnification of $\mu = 26.6$ (Hsiao et al. 2023a; Abdurro’uf et al. 2024). We show the emission lines in Figure 1. Note that Hsiao et al. (2023a) did not detect O III] $\lambda 1666$, which is the auroral line usually used to derive C/O. The small bump seen at this wavelength is within the noise, while we also speculate the bump can include contributions from both O III] $\lambda 1666$ and He II $\lambda 1640$, which are blended in the prism data. Future NIRSpec grating spectroscopy could detect and resolve these features.

MIRI Medium Resolution Spectrograph (MRS) (Wells et al. 2015; Argyriou et al. 2023) observed MACS0647–JD1 using integral field units (IFU) spectroscopy, covering all A, B and C components. The observations were conducted with two MRS bands, including SHORT and LONG, spanning $4.90\text{--}5.74 \mu\text{m}$ and $6.53\text{--}7.65 \mu\text{m}$ for channel 1, respectively. Exposure times

were 4.2 hours in each band. MIRI spectroscopic data are processed with JWST pipeline version 1.13.4 and context 1215 of the Calibration Reference Data System (CRDS). Details of the MIRI data reduction can be found in Hsiao et al. (2024). [O III] $\lambda 4960, \lambda 5008$ was detected in the SHORT band with a line flux of $(226 \pm 21) \times 10^{-19} \text{ erg s}^{-1} \text{ cm}^{-2}$, and H α was detected in the LONG band with a line flux of $(90 \pm 10) \times 10^{-19} \text{ erg s}^{-1} \text{ cm}^{-2}$ (Hsiao et al. 2024). Note that H β was not detected given the short exposure time. Throughout this article, assuming no dust, we adopt $H\beta = H\alpha/2.76$ for Case B recombination, consistent with the measurement of $H\alpha / H\gamma = 5.5 \pm 0.7$ in Hsiao et al. (2024). Hsiao et al. (2024) and Abdurro’uf et al. (2024) estimate $T_e([\text{O III}]) = 17000 \pm 1000 \text{ K}$ and $\log(n_e) = 2.9 \pm 0.5$ (see also §3), respectively, leading to a theoretical ratio of $H\alpha/H\gamma = 5.84$, which is also within the uncertainties of the measured value of 5.5 ± 0.7 .

2.2. NIRSpec spectroscopy normalized to MIRI MRS

In the MIRI MRS, JD1 A+B are both covered by the IFU, and the line flux measurements are integrated over a $0'.25$ aperture, with a correction for the aperture losses (see §3.1.1 in Hsiao et al. 2024). However, for the slitlet spectroscopy NIRSpec MSA, the slits did not fully cover JD1 A+B. In order to account for the line ratios between MIRI ([O III] $\lambda 5008$) and NIRSpec (C III] $\lambda\lambda 1907, 1909$ and [O III] $\lambda 4363$), we follow a similar approach as in Hsiao et al. (2024) to correct for the flux losses.

Hsiao et al. (2023a) measured NIRCcam photometry of MACS0647–JD within apertures of $r = 0.25''$, including aperture corrections. We integrate the NIRSpec stacked spectra over both F200W and F444W filters, which are the filters that cover C III] $\lambda\lambda 1907, 1909$ and [O III] $\lambda 4363$, respectively. We measure 189 nJy and 105 nJy for the stacked spectrum in the bandpass of F200W and F444W (with JD1 magnification $\mu = 8$), respectively. The different correction factors for C III] $\lambda\lambda 1907, 1909$ and [O III] $\lambda 4363$ might be due to the blue and red nature of the spectrum for JDA and JDB. Then the correction between the fluxes integrated with the NIRSpec prism is multiplied to match the NIRCcam aperture photometry to correct for slit losses and apply other factors as needed to correct for magnification.

We also estimate line ratios of C III] $\lambda\lambda 1907, 1909 / [\text{O III}] \lambda 5008 = 0.11 \pm 0.01$ and [O III] $\lambda 5008 / \lambda 4363 = 40 \pm 5$. The measurements and the properties used are organized in Table 1.

3. METHOD AND RESULT

In order to obtain C/O, we first assume that the carbon abundance can be inferred from the higher excita-

⁵ <https://github.com/gbrammer/msaexp>

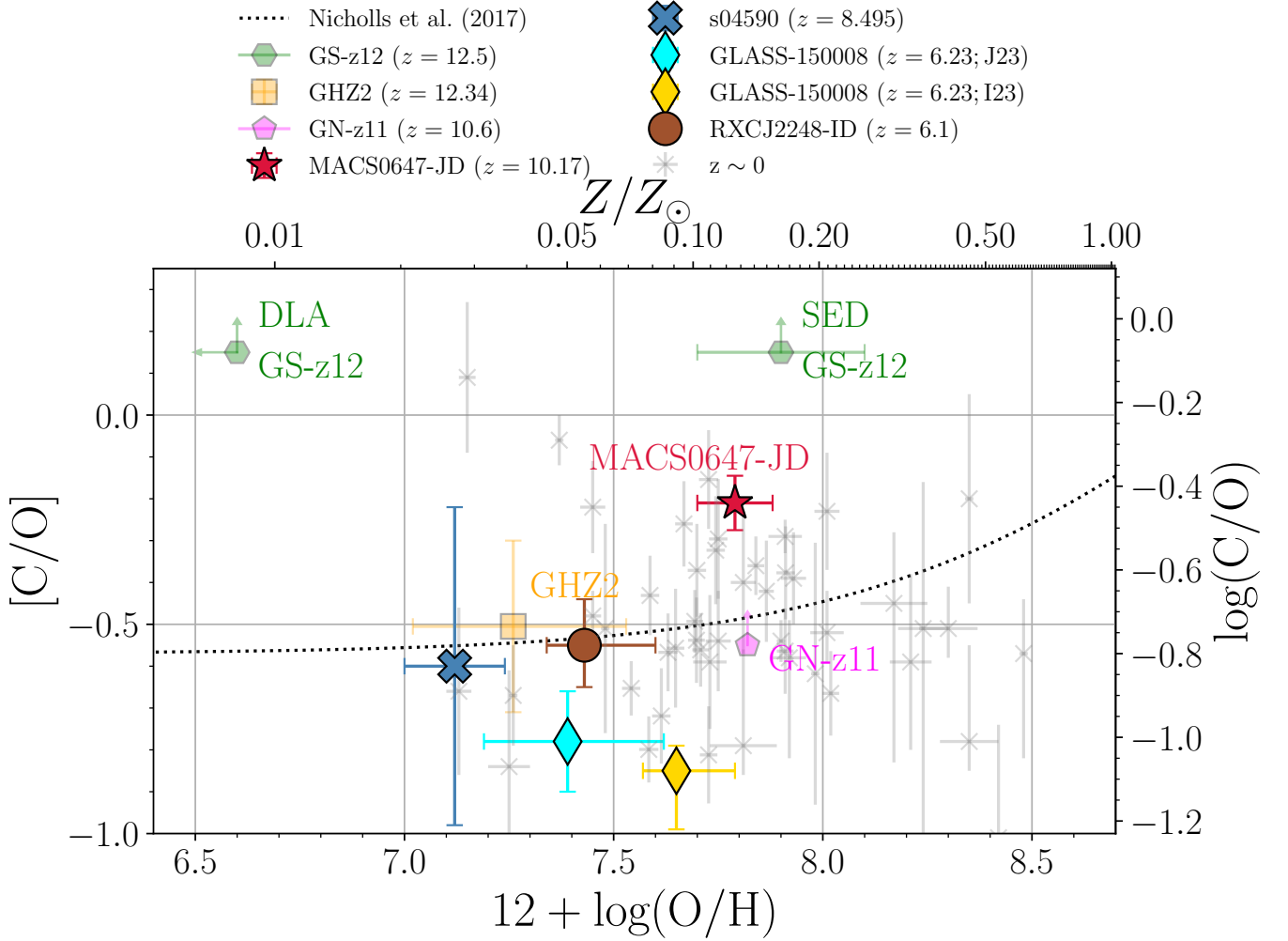


Figure 2. Abundance ratios $[C/O]$ (relative to solar) and $12 + \log(O/H)$ for MACS0647–JD compared to other galaxies. We include low- z galaxies (Berg et al. 2016; Senchyna et al. 2017; Berg et al. 2019), Milky Way Stars (Nicholls et al. 2017), as well as high- z galaxies recently studied spectroscopically with JWST: GS-z12 ($z = 12.5$; the green hexagon; D’Eugenio et al. 2023), GN-z11 ($z = 10.6$; the magenta pentagon; Cameron et al. 2023), GHZ2 ($z = 12.34$; the orange square; Castellano et al. 2024), RXCJ2248–ID ($z = 6.11$; the brown circle; Topping et al. 2024), GLASS–150008 ($z = 6.23$; the cyan and the yellow diamonds; Jones et al. 2023; Isobe et al. 2023), and s04590 ($z = 8.495$; the steelblue cross; Arellano-Córdova et al. 2022). Note that galaxies at $z > 10$ in this plot, except MACS0647–JD, are derived either assuming electron temperature (Cameron et al. 2023; Castellano et al. 2024) or through SED modelling (D’Eugenio et al. 2023), displayed with partial transparency. For GS-z12, D’Eugenio et al. (2023) presented DLA metallicity for $12 + \log(O/H)$; we also show their BEAGLE SED fitting of 7.9 ± 0.2 .

tion C^{2+}/O^{2+} with an ionization correction factor (ICF; e.g., Berg et al. 2019; Castellano et al. 2024):

$$\frac{C}{O} = \frac{C^{2+}}{O^{2+}} \times \text{ICF}. \quad (1)$$

With the detected line fluxes of $[O\text{ III}]\lambda 5008$ from MIRI MRS and the auroral line $[O\text{ III}]\lambda 4363$ from NIRSspec, we obtain an electron temperature of $T_e([O\text{ III}]) = 17000 \pm 1000$ K using the PYNEB (Luridiana et al. 2015) task `getTemDen` (Hsiao et al. 2024). We then assume $C\text{ III}]\lambda\lambda 1907, 1909$ has the same electron temperature as $[O\text{ III}]\lambda 5008$.

For the electron density, we adopt $\log(n_e) = 2.9 \pm 0.5$ derived by Abdurro’uf et al. (2024) based on resolved $[O\text{ II}]\lambda\lambda 3727, 3729$ assuming a uniform density model. (See §4.2 for future prospects on measuring electron densities in higher-ionization zones from different lines.) Note that the electron density does not significantly affect our result, with $\log(C/O)$ changing by < 0.01 when varying $\log(n_e)$ between 2.9 ± 0.5 . As a result, ionic abundances of O^{2+}/H^{2+} and C^{2+}/H^{2+} can be obtained using the task `getIonAbundance`.

For the ICF, we follow the calibration from Berg et al. (2019). With a $\log(U) = -1.9$ from $[\text{O III}] \lambda 5008 / [\text{O II}] \lambda 3727$ and metallicity $Z = 0.1 Z_{\odot}$ (Hsiao et al. 2024), we estimate an ICF of 1.10 ± 0.04 . Therefore, after the ICF correction, we obtain $\log(\text{C/O}) = -0.44^{+0.06}_{-0.07}$. These measurements are presented in Table 1.

4. DISCUSSION

4.1. A high C/O in the first 500 Myr of cosmic time?

We find a sub-solar relative carbon abundance in MACS0647–JD. Figure 2 shows the relation between carbon abundance relative to solar $[\text{C/O}]$ and metallicity $12 + \log(\text{O/H})$. We compare MACS0647–JD with previous low- z measurements and high- z galaxies recently observed with *JWST*. More metal-rich galaxies generally have higher C/O ratios, as in the case with stellar abundances in the Milky Way (Nicholls et al. 2017), shown in the black-dotted line.

Some recent galaxies at $6 < z < 10$ observed with *JWST* also present a similar trend, including s04590 at $z = 8.495$ (Arellano-Córdova et al. 2022), RXCJ2248–ID at $z = 6.11$ (Topping et al. 2024), and even lower C/O galaxies such as GLASS–150008 at $z = 6.23$ (Jones et al. 2023; Isobe et al. 2023). All of these galaxies are metal-poor ($Z < 0.1 Z_{\odot}$) and C/O-poor ($\log(\text{C/O}) < -0.75$) at $6 < z < 10$, with direct T_e measurements.

However, in the $z > 10$ regime, $[\text{O III}] \lambda 4363$ and $[\text{O III}] \lambda 5008$ are difficult to detect due to faintness and redshift, respectively. With assumed T_e , Castellano et al. (2024) estimate GHZ2 ($z = 12.34$) having a C/O as low as the $6 < z < 10$ galaxies mentioned above. For GN-z11 ($z = 10.6$), Cameron et al. (2023) estimated a lower limit suggesting higher C/O. However, GS-z12 ($z = 12.5$) hosts a significantly super-solar carbon abundance (D’Eugenio et al. 2023). They interpreted that such a high C/O ratio can be explained by the heritage of supernovae from the previous generation of first stars given the extremely low metallicity of $12 + \log(\text{O/H}) < 6.7$ (see also Maiolino & Mannucci 2019; Vanni et al. 2023).

A caveat of the $z > 10$ results is that none of those galaxies have direct metallicity or direct C/O measurements. Especially in GS-z12, the lack of Balmer lines and $[\text{O III}] \lambda 5008$ makes the O/H and C/O uncertain. D’Eugenio et al. (2023) estimated C/O based on a strong CIII] detection ($30 \pm 7 \text{ \AA}$ EW) and upper limits on OIII] $\lambda 1666$, [O II], and [Ne III]. The lines [O III] $\lambda 4363$ and [O III] $\lambda 5008$, plus most of the Balmer lines ($\text{H}\alpha$, $\text{H}\beta$, $\text{H}\gamma$, $\text{H}\delta$), are all redshifted beyond NIRSspec’s coverage, and they lack MIRI data. They estimate the gas

metallicity O/H two ways: using the properties of the local DLA (column density and dust reddening) and from BEAGLE SED fitting; we include both measurements in Fig. 2.

In this work, MACS0647–JD shows a slightly higher C/O compared with most other high- z galaxies observed with *JWST*, probably due to its higher metallicity of $12 + \log(\text{O/H}) = 7.79 \pm 0.09$. We note the C/O in MACS0647–JD is higher than the local trend found in Nicholls et al. (2017), but may be within the scatter. We emphasize that our measurement marks a milestone and the first-ever direct C/O at $z > 10$, including direct metallicity via T_e and electron density n_e , which is the most precise way to estimate the chemical abundance.

MACS0647–JD, as a whole, has a mass-weighted age of ~ 50 Myr (Hsiao et al. 2023b). A higher C/O should not be expected, if long-lived intermediate mass stars are the main source of carbon. We reckon that higher C/O might be due to a longer quiescent phase followed by a recent SFR burst. With the formation age of ~ 150 Myr (Hsiao et al. 2023b), the first AGB stars start releasing carbon in the ISM as early as 50 Myr after the onset of star formation (although the bulk of carbon is produced on timescales of several 100 Myr). Thus, the higher C/O observed, shows metal enrichment just 400 Myr after the Big Bang. There are also a few local galaxies with similar C/O and O/H studied by Berg et al. (2019), suggesting that MACS0647–JD may have undergone a very efficient and rapid burst of star formation, or has a low effective oxygen abundance yield (see Berg et al. 2019 Figure 12 therein) and could hint that very bursty star formation is important for star formation in the first few million years. Such higher C/O ratio can also originate from exotic stellar populations, including the super massive stars in proto globular clusters (Charbonnel et al. 2023) or possibly Pop III heritage if extremely low metallicity (Vanni et al. 2023; D’Eugenio et al. 2023).

In the analysis, we ignore the fact that MACS0647–JD consists of two components, JDA and JDB. We suspect that a slightly higher C/O may originate from JDB. The 2D prism spectra in Hsiao et al. (2023a) and Abdurro’uf et al. (2024) showed JDB may contribute significantly to C III] $\lambda \lambda 1907, 1909$. If JDB is indeed the culprit of high C/O, suggesting JDB is older (> 100 Myr), that would align with SED fitting findings that JDA is younger (< 50 Myr) and JDB is older (~ 100 Myr) (Hsiao et al. 2023b). Younger JDA is not expected to emit strong carbon relative to oxygen, since the long-lived intermediate mass stars should not dump carbon into the ISM yet. Therefore, CCSN could enrich oxygen shortly after the onset of star formation resulting in lower C/O instead. On the other hand,

the intermediate-mass stars may have gone through the AGB phase and released carbon into the ISM of JDB. We also refer readers to Figure 13 of Hsiao et al. (2023b), showing the extended star-formation history (SFH) in JDB, and recent bursty SFH in JDA. However, we note that it is rather difficult to model two components and disentangle them in the slit spectrum without integral field unit (IFU) spectroscopy (see §4.2), as we mentioned in §2.2.

4.2. Future Spectroscopic Observations

As discussed in §4.1, MACS0647–JD has two components A and B that are hard to disentangle as they were observed in different modes with NIRSpec MSA and MIRI MRS IFU. Therefore, NIRSpec IFU spectroscopic observations are required to further identify the origins of C III] $\lambda\lambda 1907, 1909$ and other oxygen and hydrogen lines. JWST Cycle 3 program GTO 4528 (PI Isaak) will observe MACS0647–JD with NIRSpec IFU G395M, which will detect rest-frame optical lines (2570 – 4565 Å) in JDA and JDB individually. It can also potentially detect [O III] $\lambda 4363$ in JDA and JDB and provide the direct metallicity in each clump, combined with careful modeling of A+B in the MIRI IFU spectrum. Future NIRSpec IFU observations with G235M/H (covering 1490 – 2750 Å) are essential and required to study C/O in the two components separately. G235H would resolve C III] $\lambda\lambda 1907, 1909$, delivering a more precise density in that regime rather than assuming the density derived from [O II] $\lambda\lambda 3727, 3729$ (e.g., Acharyya et al. 2019; Mingozzi et al. 2022; Topping et al. 2024). While $\log(C/O) \sim -0.44$ only changes by 0.01 when varying $\log(n_e/\text{cm}^{-3}) = 2.9 \pm 0.5$ within the uncertainties, it could change more at significantly higher densities, for example $\log(C/O) = -0.65$ for $\log(n_e/\text{cm}^{-3}) = 5$.

Not only for MACS0647–JD, but also other $z > 10$ galaxies mentioned are worth follow-up observations. For instance, MIRI would detect [O III] $\lambda 5008$ in GS-z12, which will enable more precise C/O (and also O/H) measurements. MIRI MRS observations have been obtained for GN-z11 (GO 2926; PI Colina). Deeper NIRSpec spectroscopic observations on these galaxies could deliver auroral lines and Balmer lines, leading to more accurate “direct” metallicity and C/O measurements. More generally, more galaxies at $z > 6$, or even $z > 3$ with spectroscopic data, would help answer whether C/O has a similar redshift evolution between $0 < z < 3$ as in the mass-metallicity relation and help us understand how carbon is enriched through different processes in the early universe.

5. CONCLUSIONS

In this article, we estimate the C/O abundance in a triply-lensed galaxy MACS0647–JD at $z = 10.17$. MACS0647–JD showed a bright C III] $\lambda\lambda 1907, 1909$ feature in the NIRSpec prism spectrum while no [O III] $\lambda 1666$ is detected. We estimate $\log(C/O) = -0.44^{+0.06}_{-0.07}$ using the direct electron temperature method for the first time at $z > 10$. MACS0647–JD is also the only $z > 10$ galaxy with a direct metallicity measurement. In low- z galaxies, C/O increases with metallicity $12 + \log(O/H)$. MACS0647–JD has a higher C/O ratio than local galaxies of similar metallicity, possibly due to a very efficient and rapid burst of star formation, a low effective oxygen abundance yield, or even exotic stellar populations.

We also suspect JDB, one of the component star clusters, may be the culprit of higher C/O. JDB is older, as revealed from NIRCам photometry SED fitting, suggesting it might host relatively abundant carbon since the intermediate-mass stars have started injecting carbon into the ISM. Future NIRSpec IFU observations, especially G235M/H, are essential to separate two components JDA and JDB. Additional deep spectroscopic observations of other galaxies are required to determine statistically whether a higher carbon abundance trend exists in the early universe and possibly constrain when the first stars formed.

6. ACKNOWLEDGMENTS

We appreciate Prof. Daniel Eisenstein and Prof. Dan Stark for insightful discussions.

This work is based on observations made with the NASA/ESA/CSA *James Webb Space Telescope* (JWST). The data were obtained from the Mikulski Archive for Space Telescopes (MAST) at the Space Telescope Science Institute (STScI), which is operated by the Association of Universities for Research in Astronomy (AURA), Inc., under NASA contract NAS 5-03127 for JWST. We are grateful and indebted to the 20,000 people who worked to make JWST an incredible discovery machine. These observations are associated with JWST programs GO 4246 and 1433. TH and A are funded by grants for JWST-GO-4246 provided by STScI under NASA contract NAS5-03127. TH appreciates the support from the Government scholarship to study abroad (Taiwan).

PD acknowledge support from the NWO grant 016.VIDI.189.162 (“ODIN”) and warmly thanks the European Commission’s and University of Groningen’s CO-FUND Rosalind Franklin program.

REFERENCES

- Abdurro'uf, Larson, R. L., Coe, D., et al. 2024, arXiv e-prints, arXiv:2404.16201, doi: [10.48550/arXiv.2404.16201](https://doi.org/10.48550/arXiv.2404.16201)
- Acharyya, A., Kewley, L. J., Rigby, J. R., et al. 2019, MNRAS, 488, 5862, doi: [10.1093/mnras/stz1987](https://doi.org/10.1093/mnras/stz1987)
- Arellano-Córdova, K. Z., Berg, D. A., Chisholm, J., et al. 2022, ApJL, 940, L23, doi: [10.3847/2041-8213/ac9ab2](https://doi.org/10.3847/2041-8213/ac9ab2)
- Argyriou, I., Glasse, A., Law, D. R., et al. 2023, A&A, 675, A111, doi: [10.1051/0004-6361/202346489](https://doi.org/10.1051/0004-6361/202346489)
- Asplund, M., Amarsi, A. M., & Grevesse, N. 2021, A&A, 653, A141, doi: [10.1051/0004-6361/202140445](https://doi.org/10.1051/0004-6361/202140445)
- Barkana, R., & Loeb, A. 2001, PhR, 349, 125, doi: [10.1016/S0370-1573\(01\)00019-9](https://doi.org/10.1016/S0370-1573(01)00019-9)
- Berg, D. A., Erb, D. K., Henry, R. B. C., Skillman, E. D., & McQuinn, K. B. W. 2019, ApJ, 874, 93, doi: [10.3847/1538-4357/ab020a](https://doi.org/10.3847/1538-4357/ab020a)
- Berg, D. A., Pogge, R. W., Skillman, E. D., et al. 2020, ApJ, 893, 96, doi: [10.3847/1538-4357/ab7eab](https://doi.org/10.3847/1538-4357/ab7eab)
- Berg, D. A., Skillman, E. D., Henry, R. B. C., Erb, D. K., & Carigi, L. 2016, ApJ, 827, 126, doi: [10.3847/0004-637X/827/2/126](https://doi.org/10.3847/0004-637X/827/2/126)
- Böker, T., Beck, T. L., Birkmann, S. M., et al. 2023, PASP, 135, 038001, doi: [10.1088/1538-3873/acb846](https://doi.org/10.1088/1538-3873/acb846)
- Brammer, G., Strait, V., Matharu, J., & Momcheva, I. 2022, grizli, 1.5.0, Zenodo, doi: [10.5281/zenodo.6672538](https://doi.org/10.5281/zenodo.6672538)
- Bunker, A. J., Saxena, A., Cameron, A. J., et al. 2023, A&A, 677, A88, doi: [10.1051/0004-6361/202346159](https://doi.org/10.1051/0004-6361/202346159)
- Bushouse, H., Eisenhamer, J., Dencheva, N., et al. 2023, JWST Calibration Pipeline, 1.9.4, Zenodo, doi: [10.5281/zenodo.7577320](https://doi.org/10.5281/zenodo.7577320)
- Cameron, A. J., Katz, H., Rey, M. P., & Saxena, A. 2023, MNRAS, 523, 3516, doi: [10.1093/mnras/stad1579](https://doi.org/10.1093/mnras/stad1579)
- Castellano, M., Napolitano, L., Fontana, A., et al. 2024, arXiv e-prints, arXiv:2403.10238, doi: [10.48550/arXiv.2403.10238](https://doi.org/10.48550/arXiv.2403.10238)
- Charbonnel, C., Schaerer, D., Prantzos, N., et al. 2023, A&A, 673, L7, doi: [10.1051/0004-6361/202346410](https://doi.org/10.1051/0004-6361/202346410)
- D'Eugenio, F., Maiolino, R., Carniani, S., et al. 2023, arXiv e-prints, arXiv:2311.09908, doi: [10.48550/arXiv.2311.09908](https://doi.org/10.48550/arXiv.2311.09908)
- Ferruit, P., Jakobsen, P., Giardino, G., et al. 2022, A&A, 661, A81, doi: [10.1051/0004-6361/202142673](https://doi.org/10.1051/0004-6361/202142673)
- Hsiao, T. Y.-Y., Abdurro'uf, Coe, D., et al. 2023a, arXiv e-prints, arXiv:2305.03042, doi: [10.48550/arXiv.2305.03042](https://doi.org/10.48550/arXiv.2305.03042)
- Hsiao, T. Y.-Y., Coe, D., Abdurro'uf, et al. 2023b, ApJL, 949, L34, doi: [10.3847/2041-8213/acc94b](https://doi.org/10.3847/2041-8213/acc94b)
- Hsiao, T. Y.-Y., Álvarez-Márquez, J., Coe, D., et al. 2024, arXiv e-prints, arXiv:2404.16200, doi: [10.48550/arXiv.2404.16200](https://doi.org/10.48550/arXiv.2404.16200)
- Inayoshi, K., Harikane, Y., Inoue, A. K., Li, W., & Ho, L. C. 2022, ApJL, 938, L10, doi: [10.3847/2041-8213/ac9310](https://doi.org/10.3847/2041-8213/ac9310)
- Isobe, Y., Ouchi, M., Tominaga, N., et al. 2023, ApJ, 959, 100, doi: [10.3847/1538-4357/ad09be](https://doi.org/10.3847/1538-4357/ad09be)
- Jakobsen, P., Ferruit, P., Alves de Oliveira, C., et al. 2022, A&A, 661, A80, doi: [10.1051/0004-6361/202142663](https://doi.org/10.1051/0004-6361/202142663)
- Jones, T., Sanders, R., Chen, Y., et al. 2023, ApJL, 951, L17, doi: [10.3847/2041-8213/acd938](https://doi.org/10.3847/2041-8213/acd938)
- Karakas, A. I., & Lattanzio, J. C. 2014, PASA, 31, e030, doi: [10.1017/pasa.2014.21](https://doi.org/10.1017/pasa.2014.21)
- Klessen, R. S., & Glover, S. C. O. 2023, ARA&A, 61, 65, doi: [10.1146/annurev-astro-071221-053453](https://doi.org/10.1146/annurev-astro-071221-053453)
- Kobayashi, C., Karakas, A. I., & Lugaro, M. 2020, ApJ, 900, 179, doi: [10.3847/1538-4357/abae65](https://doi.org/10.3847/1538-4357/abae65)
- Kobayashi, C., Karakas, A. I., & Umeda, H. 2011, MNRAS, 414, 3231, doi: [10.1111/j.1365-2966.2011.18621.x](https://doi.org/10.1111/j.1365-2966.2011.18621.x)
- Kuttyrev, A. S., Collins, N., Chambers, J., Moseley, S. H., & Rapchun, D. 2008, in Society of Photo-Optical Instrumentation Engineers (SPIE) Conference Series, Vol. 7010, Space Telescopes and Instrumentation 2008: Optical, Infrared, and Millimeter, ed. J. Oschmann, Jacobus M., M. W. M. de Graauw, & H. A. MacEwen, 70103D, doi: [10.1117/12.790192](https://doi.org/10.1117/12.790192)
- Luridiana, V., Morisset, C., & Shaw, R. A. 2015, A&A, 573, A42, doi: [10.1051/0004-6361/201323152](https://doi.org/10.1051/0004-6361/201323152)
- Maiolino, R., & Mannucci, F. 2019, A&A Rv, 27, 3, doi: [10.1007/s00159-018-0112-2](https://doi.org/10.1007/s00159-018-0112-2)
- Maiolino, R., Uebler, H., Perna, M., et al. 2023, arXiv e-prints, arXiv:2306.00953, doi: [10.48550/arXiv.2306.00953](https://doi.org/10.48550/arXiv.2306.00953)
- Mingozzi, M., James, B. L., Arellano-Córdova, K. Z., et al. 2022, ApJ, 939, 110, doi: [10.3847/1538-4357/ac952c](https://doi.org/10.3847/1538-4357/ac952c)
- Nicholls, D. C., Sutherland, R. S., Dopita, M. A., Kewley, L. J., & Groves, B. A. 2017, MNRAS, 466, 4403, doi: [10.1093/mnras/stw3235](https://doi.org/10.1093/mnras/stw3235)
- Nomoto, K., Kobayashi, C., & Tominaga, N. 2013, ARA&A, 51, 457, doi: [10.1146/annurev-astro-082812-140956](https://doi.org/10.1146/annurev-astro-082812-140956)
- Planck Collaboration, Aghanim, N., Akrami, Y., et al. 2020, A&A, 641, A6, doi: [10.1051/0004-6361/201833910](https://doi.org/10.1051/0004-6361/201833910)

- Rawle, T. D., Giardino, G., Franz, D. E., et al. 2022, in Society of Photo-Optical Instrumentation Engineers (SPIE) Conference Series, Vol. 12180, Space Telescopes and Instrumentation 2022: Optical, Infrared, and Millimeter Wave, ed. L. E. Coyle, S. Matsuura, & M. D. Perrin, 121803R, doi: [10.1117/12.2629231](https://doi.org/10.1117/12.2629231)
- Rieke, G. H., Wright, G. S., Böker, T., et al. 2015, PASP, 127, 584, doi: [10.1086/682252](https://doi.org/10.1086/682252)
- Rieke, M. J., Kelly, D., & Horner, S. 2005, in Society of Photo-Optical Instrumentation Engineers (SPIE) Conference Series, Vol. 5904, Cryogenic Optical Systems and Instruments XI, ed. J. B. Heaney & L. G. Burriesci, 1–8, doi: [10.1117/12.615554](https://doi.org/10.1117/12.615554)
- Rieke, M. J., Kelly, D. M., Misselt, K., et al. 2023, PASP, 135, 028001, doi: [10.1088/1538-3873/acac53](https://doi.org/10.1088/1538-3873/acac53)
- Senchyna, P., Stark, D. P., Vidal-García, A., et al. 2017, MNRAS, 472, 2608, doi: [10.1093/mnras/stx2059](https://doi.org/10.1093/mnras/stx2059)
- Topping, M. W., Stark, D. P., Senchyna, P., et al. 2024, MNRAS, 529, 3301, doi: [10.1093/mnras/stae682](https://doi.org/10.1093/mnras/stae682)
- Vanni, I., Salvadori, S., Skúladóttir, Á., Rossi, M., & Koutsouridou, I. 2023, MNRAS, 526, 2620, doi: [10.1093/mnras/stad2910](https://doi.org/10.1093/mnras/stad2910)
- Wells, M., Pel, J. W., Glasse, A., et al. 2015, PASP, 127, 646, doi: [10.1086/682281](https://doi.org/10.1086/682281)
- Wright, G. S., Wright, D., Goodson, G. B., et al. 2015, PASP, 127, 595, doi: [10.1086/682253](https://doi.org/10.1086/682253)
- Wright, G. S., Rieke, G. H., Glasse, A., et al. 2023, PASP, 135, 048003, doi: [10.1088/1538-3873/acbe66](https://doi.org/10.1088/1538-3873/acbe66)